Available online at www.sciencedirect.com
ScienceDirect
Ceramics International 38 (2012) 619–625
CERAMICS INTERNATIONAL
www.elsevier.com/locate/ceramint

Hydrothermal synthesis of carbonate-free submicron-sized barium titanate from an amorphous precursor: Synthesis and characterization

Murat Özen [a,*], Myrjam Mertens [b], Jan Luyten [b], Frans Snijkers [b], Hans D'Hondt [c], Pegie Cool [a]

[a] *Laboratory of Adsorption and Catalysis, Department of Chemistry, University of Antwerpen (UA), Universiteitsplein 1, B-2610 Wilrijk, Belgium*
[b] *Flemish Institute for Technology Research (VITO), Boeretang 200, B-2400 Mol, Belgium*
[c] *EMAT, University of Antwerpen (UA), Groenenborgerlaan 171, B-2020 Antwerpen, Belgium*

Received 12 June 2011; received in revised form 22 July 2011; accepted 23 July 2011
Available online 29th July 2011

Abstract

In this paper, the amorphous barium titanate precursor was prepared by the peroxo-hydroxide method and post-treated by various drying procedures, such as: room temperature drying, room temperature vacuum drying and vacuum drying at 50 °C. The objective in the latter two treatments was to increase the Ti–O–Ba bonds of the precursor. The post-treated precursors were compared with the untreated (i.e., 'wet') precursor. Also, a barium titanate precursor was prepared by an alkoxide route. Afterwards, the precursors were hydrothermally treated at 200 °C in a 10 M NaOH solution. Vacuum drying of the precursor seemingly promoted the formation of Ti–O–Ti bonds in the hydrothermal end-product. The low Ba:Ti ratio (0.66) of the alkoxide-route prepared precursor lead to a multi-phase hydrothermal product with $BaTiO_3$ as the main phase. In contrast, phase pure $BaTiO_3$, i.e. without $BaCO_3$ contamination, was obtained for the precursor which was dried at room temperature. Cube-shaped and highly crystalline $BaTiO_3$ particles were observed by electron microscopy for the hydrothermally treated peroxo-hydroxide-route prepared precursor.

Keywords: A. Powders: chemical preparation; B. Electron microscopy; B. X-ray methods; D. $BaTiO_3$ and titanates; IR/Raman spectroscopy

1. Introduction

A large number of studies on the preparation of barium titanate ($BaTiO_3$) have been carried out since the discovery of its ferroelectric properties in 1940s. $BaTiO_3$ is widely utilized in the manufacture of multilayer capacitors, and electro-optic devices because of its high dielectric permittivity. Barium titanate ceramics are also used in other applications, which include sensors and thermistors with positive temperature coefficient of resistivity (PTCR effect) [1–3].

Hydrothermal synthesis has several advantages over methods like coprecipitation, sol–gel, and solid-state reactions [4–6]. Hydrothermal processes have attracted extensive interest due to various advantages. Particle morphology, phase composition and surface chemical properties are some advantages of this technique. Hydrothermal processes are under great interest for the production of ceramic powders with varying morphologies and sizes [5,7–10]. One of the main issues in the synthesis of $BaTiO_3$ is the problem of carbonate formation during the synthesis and/or due to process conditions. Electrical and other important properties of $BaTiO_3$ are largely affected by carbonates. High temperature (>1100 °C) sintering of ceramic materials is necessary for industrial applications. However, impurities such as alkali metals and carbonates are highly detrimental for further industrial applications. Especially carbonates cause, what is called in literature, bloating effect during high temperature sintering of $BaTiO_3$ whereby intergranular pores are formed which reduce the density and integrity of the material.

Carbonates are present as barium carbonate ($BaCO_3$). Different procedures were suggested for removing $BaCO_3$ such as high temperature treatments and diluted acid washing. Each treatment has its down side. The high temperature treatments intend the removal of $BaCO_3$ by decomposition into BaO and CO_2 above 800 °C, however, coarsening and agglomeration is the result of the temperature treatment. Diluted acid washing of $BaTiO_3$ is also effective in the removal of $BaCO_3$, but the disadvantage of this method is the leaching of barium ions from the surface of the ceramic material [11].

* Corresponding author. Tel.: +32 03 2652380; fax: +32 03 2652374.
E-mail address: Murat.Ozen@ua.ac.be (M. Özen).

0272-8842/$36.00
doi:10.1016/j.ceramint.2011.07.051

The development of superconducting magnets with strong magnetic field equipment made possible the investigation of alignment or texturing of ceramic materials with feeble diamagnetic susceptibilities, such as $BaTiO_3$ [12], ZnO [13,14], TiO_2 [15,16], $Bi_4Ti_3O_{12}$ [12,17] and α-Al_2O_3 [18,19]. One of the requirements for alignment in a strong magnetic field of such materials is the particle size. Micron-sized or submicron-sized non-agglomerated particles are believed to aid the alignment process and hence increase the material's properties by the formation of near single-crystal like properties [13].

The research reported here is the synthesis of carbonate-free submicron $BaTiO_3$ by a facile hydrothermal synthesis. An amorphous peroxo-precursor was prepared for the hydrothermal synthesis at 200 °C for 24 h in a 10 M NaOH solution. The precursor was pre-treated: (a) dried at room temperature, henceforth just called dried; (b) RT (room temperature) vacuum dried, and (c) vacuum dried at 50 °C. The respective hydrothermal products were characterized by spectroscopic and X-ray techniques. For comparison, precursor materials were also prepared by the alkoxide route with titaniumisopropoxide and barium acetate.

2. Materials and methods

2.1. Instrumental

High-pressure and high-temperature hydrothermal reactions were performed in a stainless steel high-pressure reactor from Berghof (Germany).

Scanning electron micrographs (SEM) of the produced materials were obtained on a JEM-5510 with a resolution of 3.5 nm and equipped with an Inca X-ray microanalysis (EDX) unit enabling surface morphology studies and identification of the elements present at the surface, which was coated with gold for optimal imaging. The samples for high-resolution transmission electron microscopy (HRTEM) were prepared by crushing the powder sample in ethanol and depositing it on a holey carbon grid. HRTEM studies were performed using a Tecnai G2 electron microscope.

FT-Raman spectroscopy measurements were performed on a Nicolet Nexus 670 bench equipped with a InGaAs detector in a 180° reflective sampling configuration using a 1064 nm ND:YAG laser.

The infrared spectra were measured with a Nicolet FTIR Nexus spectrometer containing a DRIFT (diffuse reflectance infrared Fourier-transform) cell. The samples were grounded and 'diluted' (2 wt%) with KBr, as it is transparent in the mid-infrared (400–4000 cm^{-1}) region. Transmission IR was measured for liquid samples which were measured by one droplet of the liquid suspension on a KBr pellet.

TGA (thermogravimetric analysis) measurements were performed on a TGA/SDTA 851^e SF/1100 °C with a MT1 microbalance. The samples were heated in an alumina crucible (70 μl capacity) from 30 °C to 900 °C with a heating rate of 5 °C min^{-1} under O_2- or N_2-flow. DTG figures presented here were weight-normalized (1 min^{-1} vs. °C). SDTA (Single Differential Thermal Analysis) measurements were performed in an alumina crucible (70 μl capacity) with a perforated lid from 30 to 900 °C with a heating rate of 5 °C min^{-1} under O_2- or N_2-flow. Corrections were made by measuring an empty crucible at identical measuring conditions. The obtained SDTA data were converted to a DSC-signal by the formula DSC [mW] = K [mW °C^{-1}]. SDTA [°C] with $K = (\Delta H_{metal} \cdot m_0)/F_{peak,SDTA}$ and ΔH_{metal} the heat of fusion for three selected metals (In, Ag and Al), m_0 is the sample (metal) weight, and $F_{peak,SDTA}$ the integral of the SDTA peak of the respective metals. The resulting figures will be, henceforth, simply called 'SDTA–DSC' with the coordinate-axis normalized to the sample size (mW g^{-1} vs. °C).

Elemental analysis with electron probe microanalysis (EPMA) was carried out on a JEOL JXA-733 apparatus.

X-ray diffraction patterns (XRD) were collected with a PANanalytical X'Pert PRO MPD diffractometer using a Ni-monochromator and Cu K_α radiation (λ = 0.1540598 nm).

2.2. Starting materials and reagents

Amorphous peroxo-precursor was prepared with the following reagents: $BaCl_2$ (≥99.0%, Fluka), $TiCl_4$ (99.9%, Acros, Belgium), H_2O_2 (35% solution in water, Acros, Belgium), and NH_4OH (28–30 wt%, Acros, Belgium). For the alkoxide procedure following reagents were used: titanium(IV)isopropoxide $Ti[OCH(CH_3)_2]_4$ (97%, Sigma–Aldrich, Belgium), barium acetate $(CH_3COO)_2Ba$ (ACS reagent, 99%, Sigma–Aldrich, Belgium), ethanol (p.a., Merck), acetylacetonate (2,4-pentadione, 99+%, Acros, Belgium), KOH (85%, Acros, Belgium), NaOH (98.5%, Acros, Belgium). The hydrothermal reactions were performed in a 10 M NaOH solution (extra pure, pellets, Acros). All reactions were done in demi(demineralised)-water.

2.3. Synthesis

The synthesis procedure for the amorphous peroxo-precursor was adapted and modified [20]. $BaCl_2$ was dissolved in demi-water. $TiCl_4$ was added to this solution under vigorous stirring whereby a semi-transparent white coloured suspension was formed. After the addition of hydrogen peroxide, the solution's colour (pH = 1.2) turned deep red which indicated the formation of peroxo-complexes. This suspension was stirred for about 30 min to ensure a homogeneous mixture. Coprecipitation of metal-hydroxides in aqueous solutions is initiated by solubility change depending on pH [21]. Therefore, peroxo-hydroxide barium titanate was precipitated by the addition of the basic precipitating agent NH_4OH till pH 10.1 ± 0.2, accompanied by a colour change of the suspension from deep red to non-transparent milky pale green. After washing of the precipitated product with demi-water via centrifugation a 'wet' amorphous peroxo-precursor was obtained. The amorphous precursor was: (a) dried, (b) RT vacuum dried, and (c) vacuum dried at 50 °C. Afterwards, the amorphous precursors were hydrothermally treated in a 10 M NaOH solution at 200 °C for 24 h. The hydrothermal product was washed with demi-water and dried at 60 °C for at least 24 h.

The alkoxide synthesis procedure is described elsewhere [22,23]. Titanium(IV)isopropoxide was added to acetylacetonate at a ratio of 1:1 and diluted with ethanol at a Ti:ethanol ratio of 1:10. The titaniumisopropoxide and barium acetate solutions were mixed with a molar ratio Ba:Ti of 2. To increase the pH level to about 12 and hence initiate condensation KOH was added to the Ba–Ti mixture. Afterwards, the precursor was hydrothermally treated at 200 °C for 24 h in a 10 M NaOH solution.

3. Results and discussion

3.1. Amorphous precursor

The infrared measurements of the amorphous powders are depicted in Fig. 1. The transmission infrared spectroscopy of the amorphous precursor suspension (Fig. 1a) shows, as expected, intense NH_3 and carbonate bands at, respectively, ~1630 cm^{-1} (N–H bending vibrations) and ~1400 cm^{-1} (C–O stretching vibrations). After centrifugation of the suspension and washing with demi-water, the precursor was dried, RT vacuum dried and vacuum dried at 50 °C. The objective in these treatments was to strengthen the Ti·O·Ba bonds and investigate the overall stability of the precursor. The macro structure of one selected precursor in SEM has typical gel morphology (Fig. 8a). Typical infrared bands for barium titanate (○) are located at 573 cm^{-1}, 717 cm^{-1} and 831 cm^{-1} in the DRIFT spectrum (Fig. 1e). The infrared bands at 860 cm^{-1}(shoulder band), 1056 cm^{-1}, 1550 cm^{-1} and 1360 cm^{-1} correspond to carbonates (□). The region between 1360 and 1620 cm^{-1} (Fig. 1a–d) is believed to be the result of the complex interaction between –CO and –N–H [24]. Different complexes such as ammonium-carbonate, -bicarbonate, -carbamate, and diammonium carbondioxide are possible. Therefore the multiple ν(CO) stretching vibrations seen in Fig. 1 can be attributed to these various ammonium carbonate complexes. The vacuum treatment of the precursor resulted in a decrease of the band at ~1620 cm^{-1} which can be assigned to the N–H bending vibration of NH_4^+. The carbonate band at ~1360 cm^{-1} is strongly present in all samples.

Beside the band at 900–1000 cm^{-1} Raman shift, which are attributed to ammonium carbonate complexes [25], neither crystalline $BaTiO_3$ (100–800 cm^{-1}) nor other crystalline materials are observed in the Raman spectra (not shown). However, X-ray diffraction measurements (Fig. 2a and b) of the amorphous precursor show diffraction patterns of $BaCO_3$ (JCPDS # 01-071-4900) on top of broad lines of the amorphous phase. $BaCO_3$ is a well-known contamination in $BaTiO_3$ [11,26]. $BaCO_3$ formation can be explained by the presence of carbonates in the precursor material and the reaction thereof with Ba^{2+} in solution.

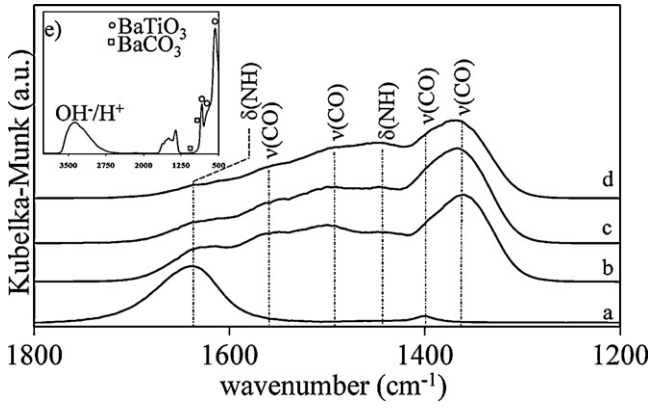

Fig. 1. Transmission infrared spectroscopy of: (a) untreated ('wet') precursor. DRIFT spectra of the amorphous precursor: (b and e) dried, (c) vacuum dried, (d) vacuum dried at 50 °C.

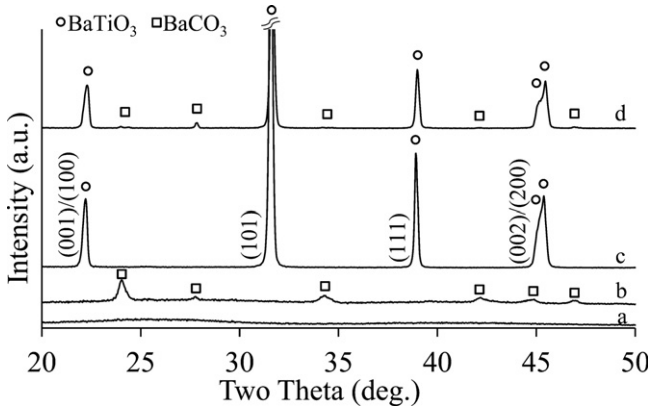

Fig. 2. X-ray diffractions of: (a) dried precursor, (b) vacuum dried precursor, (c) hydrothermal product of the dried precursor, (d) hydrothermal product of the untreated ('wet') precursor.

The peroxo-hydroxide method has been investigated extensively in literature [20,27]. The composition of the precursor material can be described either as a peroxo-hydrous oxide such as $BaZrO_2(O)_2{\cdot}6H_2O$ [28], or as a peroxo-hydroxide with the general formula $Ba_2M_2O_5(OH)_6$, with M = Ti, Zr or $Zr_xTi_{2(1-x)}$ [29]. The average Ba:Ti ratio of the precursors investigated here has been determined as 1.01 ± 0.05 by EPMA. The excess barium is most likely due to $BaCO_3$ as detected by DRIFT, XRD and Raman spectroscopy.

DTG measurements of an amorphous precursor (Fig. 3a) show three steps in the region 25–1000 °C: 25–200 °C due to

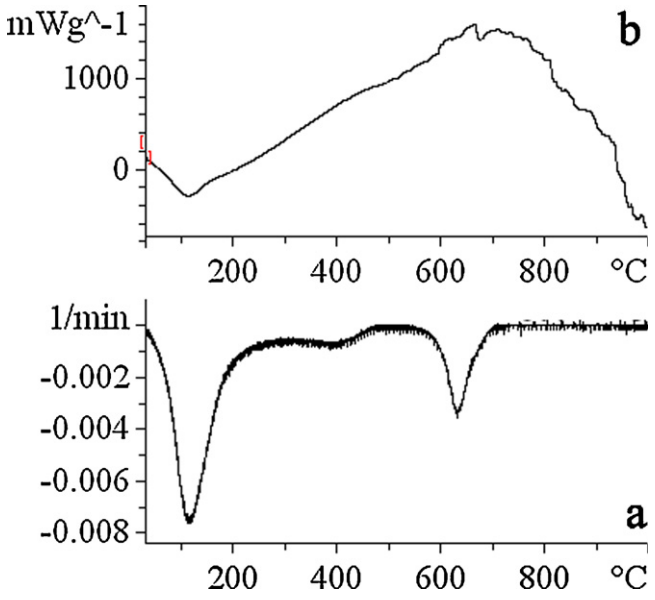

Fig. 3. DTG (a) & SDTA–DSC (b) of the dried precursor.

H_2O, ~400 °C and ~600 °C due to hydroxyl groups, and >800 °C due to $BaCO_3$. Although the precursor composition might be given as $Ba_2Ti_2O_5(OH)_6$ [20], as stated earlier, there is no conclusive answer to its exact nature.

SDTA–DSC measurement of the precursor material shows (Fig. 3b) an exothermic maximum in the region 650–700 °C which indicates the crystallization the amorphous precursor into $BaTiO_3$. The crystallization temperature is comparable and even lower than those reported in literature [30–33]. The slightly exothermic band at about ~450 °C can be attributed to peroxide and hydroxyl condensation to H_2O [26,34]. The endothermic minimum is characteristic for the evaporation of H_2O, also seen in the DTG curve (Fig. 3a).

For comparison, an amorphous precursor was also prepared by the alkoxide route. Titaniumisopropoxide and barium acetate were used as, respectively, titanium and barium source. 1 M of a mineralizer (KOH) was added in order to initiate precipitation. The initial Ba:Ti ratio was also varied: 1.1 and 2. The precipitated precursor was washed with demi-H_2O after stirring for 2 h at room temperature.

The Ba:Ti ratios of the precursor materials prepared by the alkoxide-route were determined to be 0.66 ± 0.04 (EPMA) which are far from the ideal stoichiometry for barium titanate formation. The hydrothermal products of the peroxo-hydroxide precursor and the alkoxide-precursor are discussed in the following section.

3.2. Hydrothermal treatment

The peroxo-precursors were hydrothermally treated in a 10 M NaOH solution at 200 °C for 24 h. The feedstock concentration was adjusted to 0.05 M (Ba + Ti). The precursors with different post-treatments (dried, RT vacuum dried and vacuum dried at 50 °C) and the untreated ('wet') precursor were hydrothermally processed. After centrifugation and washing with demi-H_2O (three times) the obtained hydrothermal product was dried at room temperature.

Highly crystalline $BaTiO_3$ is observed in the Raman spectra (Fig. 4a–d). The spectra are nearly similar except for the broad $BaCO_3$ band at 1060 cm^{-1} Raman shift for the sample prepared

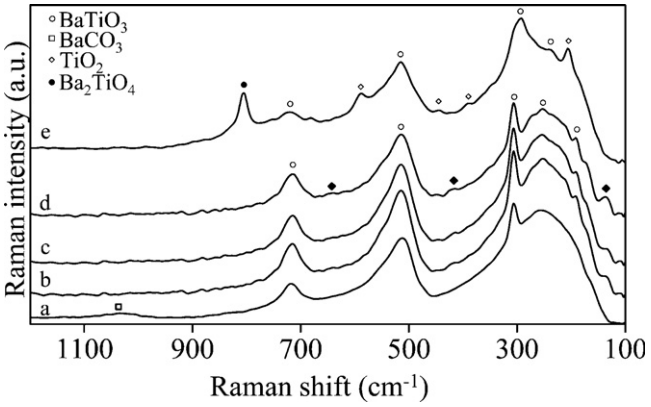

Fig. 4. Raman spectra of the hydrothermal products prepared from precursor: (a) untreated ('wet'), (b) dried, (c) vacuum dried, (d) vacuum dried at 50 °C, (e) alkoxide-precursor.

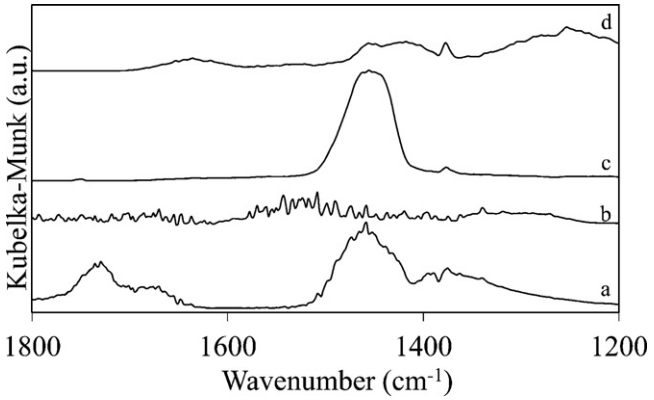

Fig. 5. DRIFT spectra of the hydrothermal products prepared from precursor: (a) untreated ('wet'), (b) dried, (c) 0.04 M and (d) 0.1 M acetic acid washing of (a).

from the untreated precursor (Fig. 4a). This difference is clearly observed in the respective DRIFT spectra (Fig. 5a–b). In the region 1300–1800 cm^{-1} several bands of carbonates (ν(C–O)) [35,36] are observed for the untreated precursor (Fig. 5a) while the same region is almost flattened for the dried precursor (Fig. 5b). X-ray diffraction pattern of the latter (Fig. 2c) reveals only $BaTiO_3$ which is partially tetragonal determined by the splitting of the ~45° 2θ diffraction line (JCPDS # 05-0626 for tetragonal barium titanate). It must be noted that X-ray diffraction techniques are not accurate for low concentrations, i.e. less than 5%.

Infrared (DRIFT) and Raman spectroscopy, with detection limits of 2% and lower, provide a better means for detecting other phases next to the $BaTiO_3$ main phase. The bands assigned with ◆ symbol in the Raman spectra (Fig. 4d) could be attributed to layered titanates [37,38]. Layered titanate bands partially overlap with those of $BaTiO_3$ and are most intense in the case of the hydrothermal product prepared from the precursor which was vacuum dried at 50 °C (Fig. 4d). Increasing the vacuum drying temperature (50 °C) promoted the formation of Ti–O–Ti bonds which could have resulted in these layered titanates. However, the latter was not detected by X-ray diffraction which, again, could be due to the limitations of XRD for very low concentrations.

Both in Raman (Fig. 4a) and DRIFT (Fig. 5a) spectra carbonates are observed for the hydrothermal product prepared from the untreated precursor. A simple drying of the precursor has resulted in a carbonate-free hydrothermal product (see Figs. 4b and 5b). The DRIFT spectrum in Fig. 5a shows only H_2O vibrational bands (1800–1400 cm^{-1}). Similar results have been obtained for the vacuum treated precursors and the respective hydrothermal products (not shown).

The hydrothermal product prepared from the untreated precursor was washed with 0.04 M and 0.1 M acetic acid solutions in order to remove barium carbonate from the hydrothermally prepared $BaTiO_3$. Acetic acid was chosen in order to track the acetate anion with DRIFT. The use of HCl, for example, might leave unwanted Cl^- ions, which are harder to detect with DRIFT and Raman spectroscopy. As can be seen in the DRIFT-spectra (Fig. 5c–d), the acetic acid washing is only partially successful in removing the carbonates. Furthermore, it

is more likely that H_3CCOO^- anions from the acetic acid will be adsorbed on the surface of $BaTiO_3$. Acid washing will also cause Ba^{2+} leaching [39] from the $BaTiO_3$ surface resulting in an amorphous Ti-rich region.

The Raman spectrum of the hydrothermally treated alkoxide-precursor in a 10 M NaOH solution at 200 °C is shown in Fig. 4e. Multi-phase product is obtained from this precursor. TiO_2 and Ba_2TiO_4 phases have been detected alongside the $BaTiO_3$ main phase. From these results, it can be concluded that the alkoxide-precursor with its poor properties (see Section 3.1) resulted in a poor hydrothermal product in comparison to the peroxo-hydroxide precursor material. Similar results for the alkoxide-precursor and the respective hydrothermal product have been reported in literature [40].

Two broad areas are observed in the SDTA–DSC figure (Fig. 6b) of the hydrothermal product prepared from the room temperature dried precursor. The broad endothermic area from 30 to 350 °C is most likely due to the overlap of H_2O evaporation, tetragonal to cubic phase transition of $BaTiO_3$, and hydroxyl (OH^-)/proton (H^+) diffusion [41]. However, the broad exothermic area between 450 and 800 °C is harder to assign. Crystallization of unreacted amorphous precursor is not in order here, because if this were the case no exothermic signals should have been observed in SDTA–DSC for the same sample calcined at 550 °C, 950 °C, and 1400 °C. The same analogy can be followed for OH^-/H^+ diffusion which should not be present after calcination at 550 °C, 950 °C, and 1400 °C (Fig. 7–O_2). One possible explanation is the uptake of oxygen by the defect perovskite $BaTiO_3$. According to Hennings et al. [26] oxygen vacancies are created by the evaporation of H_2O. When comparing SDTA–DSC measured under O_2- and N_2-flow (Fig. 7), the differences are clearly observed in the temperature region 400–800 °C. Thus, the exothermic band cannot be attributed solely to hydroxyl or proton diffusion. It is more likely that the same process (oxygen uptake) takes place in each of the samples. The respective DTG figure shows (Fig. 6a) a very small relative weight loss per minute (1 min^{-1}) at ~400 °C. The combined effect of OH^-/H^+ diffusion (weight loss) and O_2-uptake (weight increase) might very well explain this small effect in DTG. Since the oxygen determination by X-ray techniques, such as EDX and EPMA, is not highly accurate, oxygen vacancies cannot be determined correctly by these elemental analysis techniques.

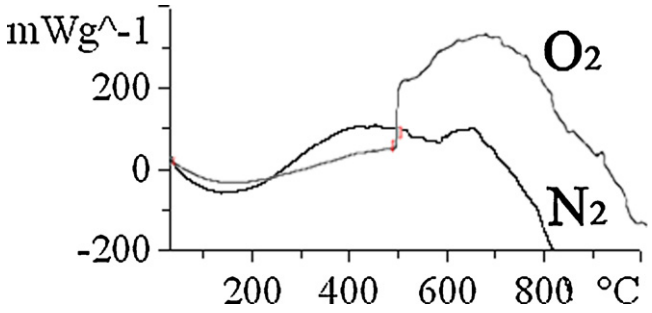

Fig. 7. SDTA–DSC of $BaTiO_3$ sintered at 1400 °C under O_2 and N_2 flow.

Scanning electron image of the hydrothermal product prepared with the dried precursor is given in Fig. 8b. Distinct cube-shaped particles are observed in SEM. EDX analysis of several spots on a particle and on several particles resulted in a Ba:Ti ratio close to unity. Certain amounts of sodium (~1 wt%), due to the use of a 10 M NaOH solution during

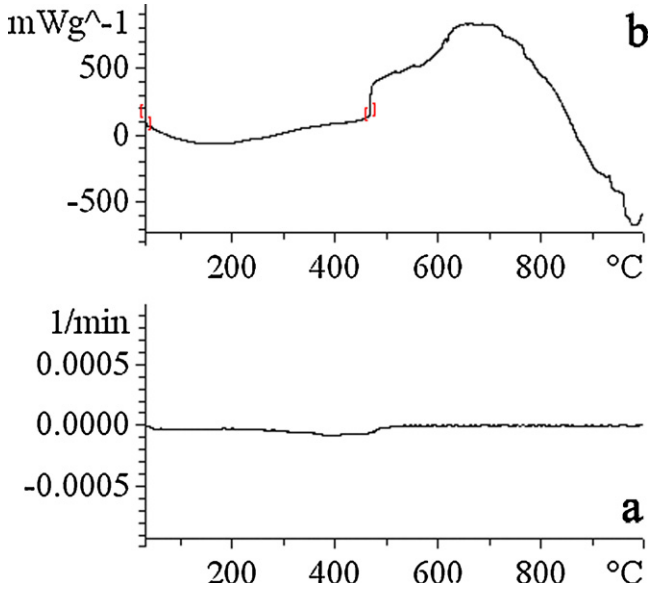

Fig. 6. DTG (a) & SDTA–DSC (b) of the hydrothermal product prepared from the dried precursor.

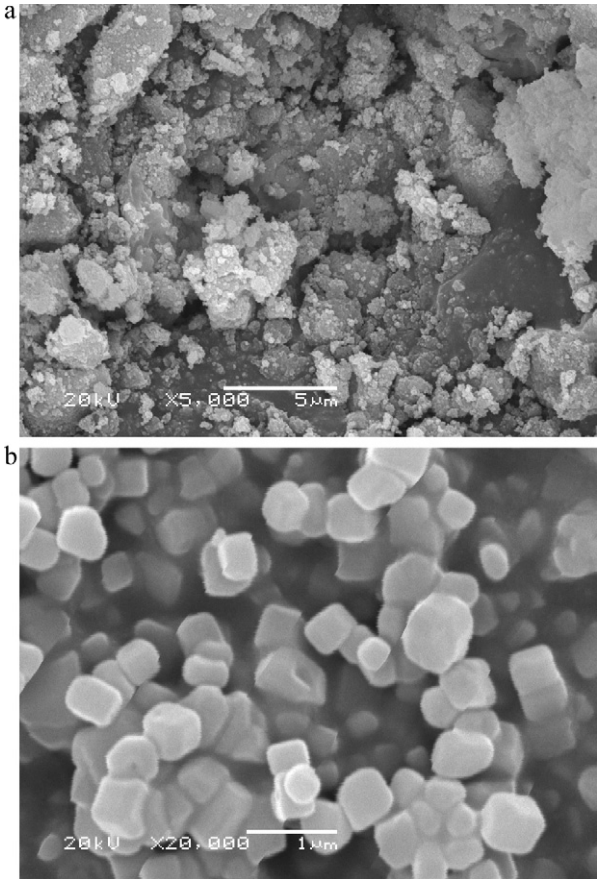

Fig. 8. Scanning electron micrograph: dried precursor (a), and the respective hydrothermal product (b).

the hydrothermal reaction, has also been detected, but not continuously. The low amounts, if any present, makes the detection of sodium very difficult. High resolution transmission electron measurement (not shown) of a single particle confirms the highly crystalline and defect-free nature of $BaTiO_3$.

4. Conclusion

The amorphous peroxo-precursor study showed that it has a very good stability, in comparison with the precursor prepared by the alkoxide route. XRD confirmed the amorphous character of the peroxo-precursor, however, with some degree of witherite $BaCO_3$ formed especially for the vacuum treated precursors. The region of 1360–1620 cm^{-1} in the infrared spectrum is believed to be the result of the complex interaction between –C–O and –N–H which have reacted into various ammonium carbonates. These complexes are believed to have been incorporated in the hydrothermal product prepared from the untreated 'wet' precursor. Washing of the hydrothermal product with acetic acid was only partially successful in removing carbonates. Remnants of the acetate anion were detected by DRIFT. Additional steps, such as calcination, are needed to remove the organic groups. However, a simple drying step of the precursor resulted in the removal of carbonates. Cube-shaped and highly crystalline $BaTiO_3$ was observed by electron microscopy and X-ray powder diffraction techniques for the hydrothermal product prepared from the dried precursor.

Literature data are not in full agreement of the composition of the precursor material prepared by the peroxo-method. Hydrous oxide or peroxo-hydroxide $[Ba_2Ti_2O_5(OH)_6]$ has been suggested as the composition of the precursor. The crystallization of the amorphous precursor into $BaTiO_3$ occurred at a temperature of 650–700 °C (TGA/SDTA–DSC) which is comparable and even lower than values presented in literature. Comparison of SDTA–DSC measurements under O_2- and N_2-flow showed a significant decrease of the exothermic area under inert atmosphere which confirmed the oxygen defect nature of the hydrothermally produced $BaTiO_3$.

Acknowledgements

This work has been performed within a project of the Flemish Institute for the Promotion of Scientific Technological Research in Industry (IWT) under contract SBO-PROMAG (60056). The research is also performed within the framework of a GOA-BOF project supported by the University of Antwerpen.

References

[1] J.C. Burfoot, Ferroelectrics: An Introduction to the Physical Principles, Van Nostrand, London, Princeton, NJ, 1967.
[2] M.E. Lines, A.M. Glass, Principles and Applications of Ferroelectrics and Related Materials, OUP, Oxford, 2001.
[3] R. Smoluchowski, N. Kurti, Ferroelectric Crystals, Pergamon Press, Oxford, 1962.
[4] M. Yoshimura, K. Byrappa, Hydrothermal processing of materials: past, present and future, J. Mater. Sci. 43 (7) (2008) 2085–2103.
[5] W.L. Suchanek, R.E. Riman, Hydrothermal synthesis of advanced ceramic powders, Adv. Sci. Technol. 45 (2006) 184–193.
[6] D.H. Yoon, S.S. Ryu, Solid-state synthesis of nano-sized $BaTiO_3$ powder with high tetragonality, J. Mater. Sci. 42 (17) (2007) 7093–7099.
[7] L. Zhou, R. Yu, K. Zhu, J. Yao, X. Xing, D. Wang, W. Xu, Preparation of plank-like $BaTiO_3$ by hydrothermal soft chemical process from layered titanates precursors, Key Eng. Mater. 336–338 (2007) 66–68.
[8] T.J. Yosenick, D.V. Miller, R. Kumar, J.A. Nelson, C.A. Randall, J.H. Adair, Synthesis of nanotabular barium titanate via a hydrothermal route, J. Mater. Res. 20 (4) (2005) 837–843.
[9] E. Suvaci, J. Anderson, G.L. Messing, J.H. Adair, Hydrothermal synthesis of tabular perovskite particles, Key Eng. Mater. (2002) 163–166, 206–2.
[10] J. Moon, M.L. Carasso, H.G. Krarup, J.A. Kerchner, J.H. Adair, Particle-shape control and formation mechanisms of hydrothermally derived lead titanate, J. Mater. Res. 14 (3) (1999) 866–875.
[11] C.C. Li, J.H. Jean, Dissolution and dispersion behavior of barium carbonate in aqueous suspensions, J. Am. Ceram. Soc. 85 (12) (2002) 2977–2983.
[12] K. Watari, W.W. Chen, Y. Kinemuchi, T. Tamura, K. Miwa, Fabrication of textured ferroelectric ceramics by magnetic alignment via gelcasting, J. Eur. Ceram. Soc. 27 (2–3) (2007) 655–661.
[13] Y. Sakka, T.S. Suzuki, Textured development of feeble magnetic ceramics by colloidal processing under high magnetic field, J. Ceram. Soc. Jpn. 113 (1313) (2005) 26–36.
[14] S. Tanaka, A. Makiya, Z. Kato, K. Uematsu, *c*-Axis oriented ZnO formed in a rotating magnetic field with various rotation speeds, J. Eur. Ceram. Soc. 29 (5) (2009) 955–959.
[15] A. Makiya, Y. Kusumi, S. Tanaka, Z. Kato, N. Uchida, K. Uematsu, T. Kimura, K. Kitazawa, Grain oriented titania ceramics made in high magnetic field, J. Eur. Ceram. Soc. 27 (2–3) (2007) 797–799.
[16] T.S. Suzuki, Y. Sakka, Fabrication of textured titania by slip casting in a high magnetic field followed by heating, Jpn. J. Appl. Phys. 41 (11A) (2002) L1272–L1274.
[17] A. Makiya, D. Kusano, S. Tanaka, N. Uchida, K. Uematsu, T. Kimura, K. Kitazawa, Y. Doshida, Particle oriented bismuth titanate ceramics made in high magnetic field, J. Ceram. Soc. Jpn. 111 (9) (2003) 702–704.
[18] T.S. Suzuki, Y. Sakka, K. Kitazawa, Orientation amplification of alumina by colloidal filtration in a strong magnetic field and sintering, Adv. Eng. Mater. 3 (7) (2001) 490–492.
[19] T.S. Suzuki, T. Uchikoshi, Y. Sakka, Control of texture in alumina by colloidal processing in a strong magnetic field, Sci. Technol. Adv. Mater. 7 (4) (2006) 356–364.
[20] B.W. Lee, S.B. Cho, Hydrothermal preparation and characterization of ultra-fine BaTiO3 powders from amorphous peroxo-hydroxide precursor, J. Electroceram. 13 (1–3) (2004) 379–384.
[21] J. Livage, M. Henry, C. Sanchez, Sol–gel chemistry of transition-metal oxides, Prog. Solid State Chem. 18 (4) (1988) 259–341.
[22] J. Moon, E. Suvaci, T. Li, S.A. Costantino, J.H. Adair, Phase development of barium titanate from chemically modified-amorphous titanium (hydrous) oxide precursor, J. Eur. Ceram. Soc. 22 (6) (2002) 809–815.
[23] J. Moon, J.A. Kerchner, H. Krarup, J.H. Adair, Hydrothermal synthesis of ferroelectric perovskites from chemically modified titanium isopropoxide and acetate salts, J. Mater. Res. 14 (2) (1999) 425–435.
[24] V.A. Gal'perin, A.I. Finkel'shtein, Infrared spectra of ammonium carbamate and bicarbonate, J. Appl. Spectrosc. 17 (3) (1972) 468–471.
[25] N.P. Wen, M.H. Brooker, Ammonium carbonate, ammonium bicarbonate, and ammonium carbamate equilibria – a Raman study, J. Phys. Chem. 99 (1) (1995) 359–368.
[26] D.F.K. Hennings, C. Metzmacher, B.S. Schreinemacher, Defect chemistry and microstructure of hydrothermal barium titanate, J. Am. Ceram. Soc. 84 (1) (2001) 179–182.
[27] B.W. Lee, Synthesis and characterization of compositionally modified PZT by wet chemical preparation from aqueous solution, J. Eur. Ceram. Soc. 24 (6) (2004) 925–929.
[28] G. Pfaff, A novel reaction-path to barium zirconates by the decomposition of peroxide precursors, Mater. Lett. 24 (6) (1995) 393–397.
[29] B.W. Lee, S.B. Cho, Preparation of $BaZr_xTi_{1-x}O_3$ by the hydrothermal process from peroxo-precursors, J. Eur. Ceram. Soc. 25 (12) (2005) 2009–2012.

[30] P.F. Yu, B. Cui, Q.Z. Shi, Preparation and characterization of $BaTiO_3$ powders and ceramics by sol–gel process using oleic acid as surfactant, Mater. Sci. Eng. A: Struct. 473 (1–2) (2008) 34–41.
[31] L. Simon-Seveyrat, A. Hajjaji, Y. Emiane, B. Guiffard, D. Guyomar, Re-investigation of synthesis of $BaTiO_3$ by conventional solid-state reaction and oxalate coprecipitation route for piezoelectric applications, Ceram. Int. 33 (1) (2007) 35–40.
[32] L.B. Kong, J. Ma, H. Huang, R.F. Zhang, W.X. Que, Barium titanate derived from mechanochemically activated powders, J. Alloys Compd. 337 (2002) 226–230.
[33] S. Ghosh, S. Dasgupta, A. Sen, H.S. Maiti, Synthesis of barium titanate nanopowder by a soft chemical process, Mater. Lett. 61 (2) (2007) 538–541.
[34] S.Y. Cho, I.T. Kim, D.Y. Kim, S.J. Park, B.K. Kim, J.H. Lee, Effects of H_2O_2 on the morphology of ZrO_2 powder prepared by ultrasonic spray pyrolysis, Mater. Lett. 32 (4) (1997) 271–273.
[35] G. Socrates, Infrared and Raman Characteristic Group Frequencies – Tables and Charts, third ed., John Wiley and Sons Ltd., Chichester, 2001
[36] S.J. Chang, W.S. Liao, C.J. Ciou, J.T. Lee, C.C. Li, An efficient approach to derive hydroxyl groups on the surface of barium titanate nanoparticles to improve its chemical modification ability, J. Colloid Interface Sci. 329 (2) (2009) 300–305.
[37] P.H. Wen, H. Itoh, W.P. Tang, Q. Feng, Transformation of layered titanate nanosheets into nanostructured porous titanium dioxide in polycation solution, Micropor. Mesopor. Mater. 116 (1–3) (2008) 147–156.
[38] Q. Feng, M. Hirasawa, K. Yanagisawa, Synthesis of crystal-axis-oriented $BaTiO_3$ and anatase platelike particles by a hydrothermal soft chemical process, Chem. Mater. 13 (2) (2001) 290–296.
[39] J.H. Adair, J. Crampo, M.M. Mandanas, E. Suvaci, The role of material chemistry in processing $BaTiO_3$ in aqueous suspensions, J. Am. Ceram. Soc. 89 (6) (2006) 1853–1860.
[40] S.K. Lee, T.J. Park, G.J. Choi, K.K. Koo, S.W. Kim, Effects of KOH/BaTi and Ba/Ti ratios on synthesis of $BaTiO_3$ powder by coprecipitation/hydrothermal reaction, Mater. Chem. Phys. 82 (3) (2003) 742–749.
[41] M.H. Frey, D.A. Payne, Grain-size effect on structure and phase transformations for barium titanate, Phys. Rev. B 54 (5) (1996) 3158–3168.